Alternate raft pathways cooperate to mediate slow diffusion and efficient uptake of a sphingolipid tracer to degradative and recycling compartments

Dawei Zhang[1], Manoj Manna[2], Thorsten Wohland[2] and Rachel Kraut[3,*]

[1]Institute of Medical Biology, Agency for Science, Technology and Research (A-STAR), Singapore 138648
[2]Department of Chemistry, National University of Singapore, Singapore 117543
[3]School of Biological Sciences, Nanyang Technological University, Singapore 637551
*Author for correspondence (rskraut@ntu.edu.sg)

Accepted 3 August 2009
Journal of Cell Science 122, 3715-3728 Published by The Company of Biologists 2009
doi:10.1242/jcs.051557

Summary

Several cholesterol-dependent cellular uptake pathways involving microdomain-resident sphingolipids have been characterized, but little is known about what controls the further intracellular trafficking routes of those domains. Here, we present evidence that the uptake and intracellular trafficking of a recently described sphingolipid-binding probe, the sphingolipid binding domain (SBD) peptide, is mediated by two parallel cooperating mechanisms requiring flotillin, dynamin and cdc42, which act in concert to direct a distinct surface behavior and trafficking itinerary. Diffusion measurements of SBD at the cell surface by fluorescence correlation spectroscopy suggest that cdc42- and flotillin-associated uptake sites both correspond to domains of intermediate mobility, but that they can cooperate to form low-mobility, efficiently internalized domains. Interestingly, we find that the choice of uptake mechanism affects subsequent trafficking of SBD, as does cholesterol content. Interference with one or other uptake pathway acts as a toggle switch for the trafficking of SBD to recycling endosomes or endolysosomes, whereas both of these pathways are bypassed if cholesterol is reduced. The data are in accordance with a scenario in which SBD mirrors the trafficking response of raft-borne lipids towards a degradative or recycling target. In summary, we suggest that both the surface behavior of a cargo and its subsequent trafficking are determined by a combination of endocytic accessory proteins and the cholesterol content of different membrane compartments.

Supplementary material available online at
http://jcs.biologists.org/cgi/content/full/122/20/3715/DC1

Key words: FCS, SBD, Microdomain, Raft, Sphingolipid, Trafficking

Introduction

The discovery that many endocytic cargoes enter cells through clathrin-independent pathways has triggered interest in the identification of the endocytic machinery and membrane-trafficking itineraries of these pathways. Among these non-clathrin pathways, some are based on a constitutive internalization mechanism, whereas others are initiated by specific signals, e.g. cytokine signaling (Lamaze et al., 2001; Mayor and Pagano, 2007). However, it has been documented that some cargoes might be endocytosed through alternate or sequential pathways, dependent on cell type and treatment (Deinhardt et al., 2006; Massol et al., 2004; Sandvig et al., 2004). For example, in cells that lack clathrin or caveolae, internalization can still occur via alternative pathways. Several bacterial toxins, as well as the amyloid precursor protein (App), combine raft-mediated association at the plasma membrane with subsequent endocytosis, assisted by components common to clathrin- and/or dynamin-mediated uptake (Abrami et al., 2003; Schneider et al., 2008).

As well as determining which cargos are taken up by particular raft-associated mechanisms, it is important to understand the post-internalization trafficking routes following these entry mechanisms. It has been noted that various raft-borne endocytic cargoes are transported to different intracellular destinations. Some examples are enterotoxins such as cholera and shiga toxins, which are transported rapidly from the plasma membrane to the Golgi, and thereafter retrogradely to the endoplasmic reticulum, where toxic effects ensue (Lencer and Saslowsky, 2005). One well-studied class of raft-borne endocytic cargos are the glycosyl-phosphatidylinositol-associated proteins (GPI-APs) (Mayor and Riezman, 2004), which are thought to internalize via cdc42, into a specialized 'GEEC' compartment (Sabaranjak et al., 2002) and thereafter most probably traffic to recycling endosomes and possibly Golgi (Nichols et al., 2001). Raft-associated adaptor proteins flotillin-1 and flotillin-2, which constitute a separate internalization pathway from either caveolin or GPI-AP uptake, target partially to lysosomes (Glebov et al., 2006; Langhorst et al., 2008).

Clathrin-independent internalization phenomena are associated with plasma membrane microdomains or lipid rafts, defined functionally by their structural requirement for sphingolipids and cholesterol (Hancock, 2006). The role of cholesterol in clathrin-independent endocytosis, such as caveola formation (Hooper, 1999), is considered diagnostic for the presence of raft-mediated mechanisms. A critical level of cholesterol is required for the organization of raft-borne molecules into nanoclusters at the cell surface, estimated to be ~20-40% of the population at any given time (Goswami et al., 2008; Lasserre et al., 2008; Sharma et al., 2004). The cholesterol content in membranes has been shown to influence the integrity and functions of lipid rafts in signal transduction (Gomez-Mouton et al., 2004; Jury et al., 2007). It is also known that overload of cholesterol and sphingolipids influences the membrane trafficking of raft adaptor proteins (Pol et al., 2005)

and lipid raft constituents, as occurs in the lipid storage diseases (Pagano et al., 2000; Simons and Gruenberg, 2000).

It is obvious from all of this data that cholesterol and sphingolipids are important for the uptake and trafficking of raft-associated molecules, but the rules governing the endocytic trafficking routes of these cargoes have not yet emerged. Although distinct intracellular pathways have been noted for certain raft-mediated cargo (Le and Nabi, 2003; Payne et al., 2007; Sabharanjak et al., 2002) we do not have a clear picture of how or whether the specific machinery of uptake also affects subsequent intracellular targeting. Neither has there been any observation as yet that would link the endocytic machinery (apart from cholesterol and sphingolipids) with a particular diffusion behavior (Goswami et al., 2008; Umemura et al., 2008).

In this study, we investigate the relationship between uptake mechanism, surface behavior and endocytic targeting of the recently characterized sphingolipid and raft-interacting probe, sphingolipid binding domain (SBD), in mammalian neuroblastoma cells. SBD, a fluorescently coupled peptide consisting of the V3-loop domain of the amyloid beta peptide (Aβ) (Fantini et al., 2002), was shown to interact with a subset of glycosphingolipids, sphingomyelin and cholesterol in artificial membranes as well as with cholesterol- and sphingolipid-dependent microdomains in neurons (Hebbar et al., 2008; Steinert et al., 2008). Here, we show that SBD uptake is dependent on several different mechanisms – flotillin, cdc42, and dynamin – that have generally been viewed as independent and parallel pathways (Glebov et al., 2006; Mayor and Pagano, 2007; Sabharanjak et al., 2002). Suggestive of synergism between these mechanisms, interference with individual components only partially suppresses uptake of SBD into cells, whereas knocking out the flotillin and cdc42 pathways simultaneously nearly eliminates uptake. By contrast, drastic changes in the raft-like diffusion behavior of SBD are seen when either or both of these uptake pathways are perturbed. We also observe that knockout of either cdc42- or flotillin-mediated uptake leads to a trafficking switch, as do conditions of altered cholesterol storage. This suggests that these alternate pathways favor different subcellular itineraries that are related to cholesterol-induced changes in the intracellular targeting of sphingolipids.

Results

Kinetics of SBD internalization in SH-SY5Y neuroblastoma

The fluorescently tagged SBD (Mahfoud et al., 2002) peptide acts as a sphingolipid-interacting tracer with potential applications in the study of neurodegenerative disease (Hebbar et al., 2008; Steinert et al., 2008). For this reason, we examined the uptake characteristics and intracellular trafficking of the SBD marker in neuroblastoma SH-SY5Y cells.

We determined the kinetics of cellular internalization of SBD in SH-SY5Y cells (Fig. 1A), by normalizing the unit fluorescence intensity of internalized label at a given time point against the average unit fluorescence after complete internalization at 60 minutes. Tetramethylrhodamine (TMR)- or Oregon green (OG)-labeled SBD was added to cells at a concentration of 10 μM and the cellular fluorescence quantitatively assessed at different time points. SBD is internalized rapidly, with >80% of maximum fluorescence obtained after 15 minutes. The internalization kinetics were nearly identical between TMR- and OG-tagged SBD (Fig. 1A). After ~15 minutes of incubation, internalization of SBD-TMR and SBD-OG gave rise to discrete labeled compartments in the cytoplasm (Fig. 1B). The identity of these compartments was investigated, as described below.

SBD trafficking follows flotillin-2 and GPI-AP but not CtxB pathways

In order to determine the uptake and intracellular trafficking route of SBD in neuroblastomas, we compared its localization to commonly used endocytic markers at early time points. First, the colocalization of SBD with the known GM1-binding marker Cholera toxin B (CtxB) and the clathrin-dependent marker transferrin (Tfn)-Alexa594 was re-examined (Fig. 2A-E) under different labeling conditions to those previously used (Steinert et al., 2008). Here, loading of the cells with fluorescent label was carried out for shorter time periods (10 or 15 minutes) and on ice,

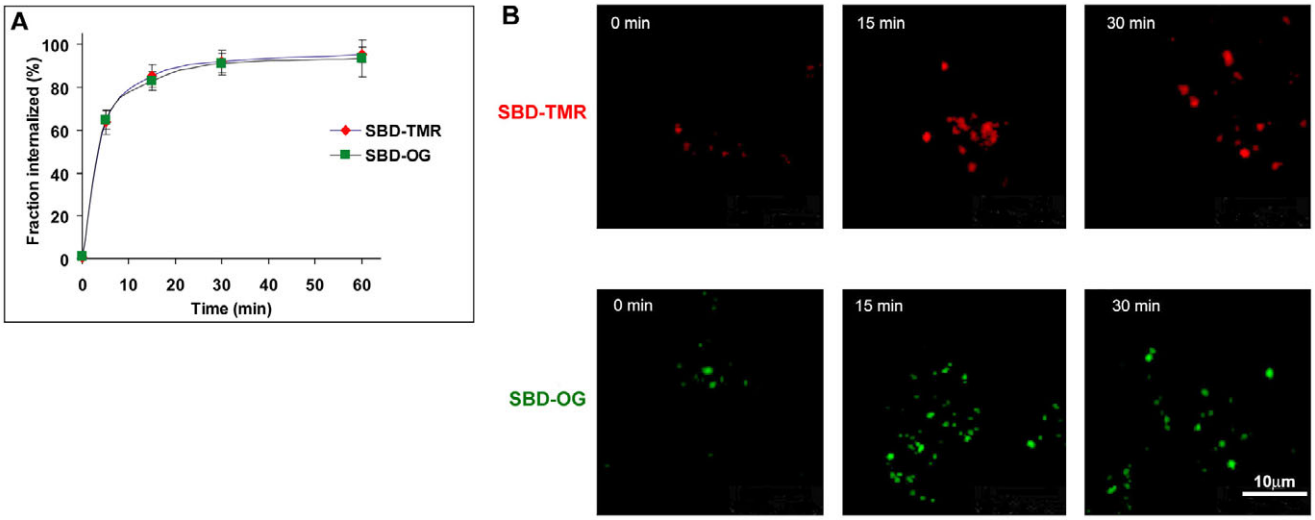

Fig. 1. Uptake rate of SBD into human neuroblastoma SH-SY5Y cells. (A) Uptake of SBD-TMR (red diamonds) and SBD-OG (green squares) into SH-SY5Y neuroblastoma over time, indicated by percent internalization, measured as average fluorescence intensity per pixel in cells being measured divided by maximum average fluorescence intensity per pixel reached after 60 minutes of chase in control cells. (B) SBD-TMR (top) and SBD-OG (bottom) uptake after 0, 15, and 30 minutes (0 time-point is defined as immediately after post-incubation washing of excess label).

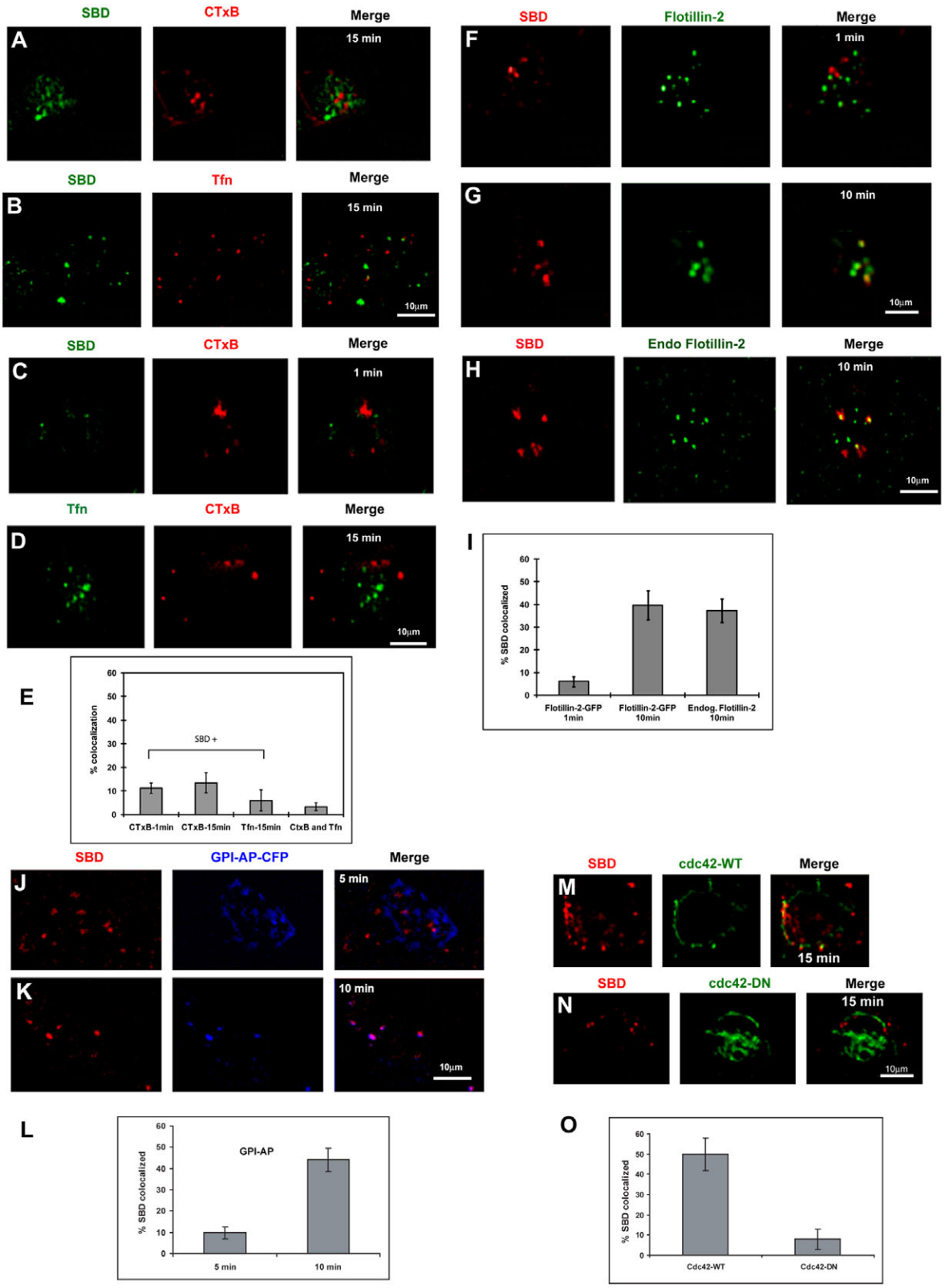

Fig. 2. Comparison of SBD localization in early sorting compartments with raft-associated labels. (A,B,C) SBD-OG colocalization with CtxB- and Tfn-Alexa594 was minimal in a sorting compartment at 15 minutes. (D) CtxB-Alexa594 colocalization with Tfn-Alexa488 was also minimal at 15 minutes. (E) Quantification of SBD colocalization (tM^{SBD}) with CtxB and Tfn, and of CtxB with Tfn. (F,G) SBD-TMR colocalized ~40% with flotillin-2–GFP, but only after 10 minutes. (H) SBD-TMR colocalized to a similar extent with endogenous flotillin-2 after 10 minutes, detected by immunofluorescence. (I) Quantification of SBD colocalization (tM^{SBD}) with flotillin-2–GFP and endogenous flotillin-2. (J,K,L) SBD-TMR colocalized (tM^{SBD}) ~45% with GPI-AP–CFP after 10 minutes. (M,N,O) SBD-TMR colocalized (tM^{SBD}) ~50% after 15 minutes with cdc42-WT–GFP but <10% with inactive cdc42-DN–GFP. Values in E, I, L and O represent means ± s.e.m.

in order to ensure synchronous uptake upon warming to 37°C, starting at time 0. CtxB labelings were carried out in the absence of antibody cross-linking, because this procedure could possibly affect uptake and subsequent trafficking behavior. Quantification of colocalization was determined by the Costes thresholding method, and reported as the thresholded Manders' coefficient for the SBD channel (tM^{SBD}; see Materials and Methods and Fig. 2E).

Due to its association with ganglioside, CtxB is expected to localize at least partially to sphingolipid-rich microdomains (Shogomori and Futerman, 2001; Wolf et al., 1998). In spite of this, SBD and CtxB colocalized very little in early endocytic vesicles and sorting compartments (1 and 15 minute time points), comparable to the colocalization of SBD with Tfn (Fig. 2A-C,E). This closely matched previous results (Steinert et al., 2008) and confirmed that these two sphingolipid-dependent markers follow distinct intracellular routes. To confirm that the low degree of colocalization was not due to CtxB following a predominantly clathrin-dependent pathway in this cell type, colocalization between CtxB and Tfn was also checked, but was found to be very low, as expected (Fig. 2D,E).

Flotillins are multiply acylated, membrane-associated scaffolding proteins involved in the assembly of non-clathrin and non-caveolar endocytic platforms of ~50-100 nm (Stuermer et al., 2001) that are largely non-overlapping with domains carrying CtxB or GPI-AP (Glebov et al., 2006; Langhorst et al., 2008). Flotillin-2 forms hetero- and homotetrameric complexes with flotillin-1, and is required for the maintenance of flotillin-1, but has a slightly different distribution from flotillin-1 (Langhorst et al., 2005; Solis et al., 2007). A flotillin-2–GFP (GFP, green fluorescent protein) transfected fusion protein (Neumann-Giesen et al., 2004; Steinert et al., 2008) and endogenous flotillin-2 were compared to SBD as a second raft-associated marker. After 1 minute, SBD showed very little colocalization with flotillin-2–GFP (presumably because flotillin-2–GFP is systemically expressed, whereas SBD is added externally), but this rose to ~40% after only 10 minutes, similar to its degree of colocalization with the endogenous flotillin-2 protein (Fig. 2F-I). Again, this confirmed earlier results with non-synchronized uptake.

To test whether the SBD is endocytosed through a similar pathway to that of the GPI-APs, which are localized partially to nanoclustered, raft-dependent domains and endocytosed through a specialized GPI-AP-enriched early endosomal compartment (GEEC) (Sabharanjak et al., 2002), we expressed cyan fluorescent protein (CFP)-tagged GPI-AP protein (GPI-AP–CFP) in SH-SY5Y cells (Keller et al., 2001). Upon addition, SBD is not coincident with GPI-AP–CFP but rapidly colocalizes (10 minutes; Fig. 2J-L), showing that SBD probably enters the GEEC pathway.

Mechanism of SBD uptake: simultaneous cdc42 and dynamin dependence

The Rho family small GTPase cdc42 mediates the endocytosis of GPI-APs via the GEEC pathway, and this process does not involve dynamin (Sabharanjak et al., 2002). To test whether cdc42 also has a role in SBD endocytosis, we expressed wild-type and dominant-negative (DN, $cdc42^{N17}$) forms of GFP-tagged cdc42 in SH-SY5Y cells, and checked for both colocalization and a change in the uptake of SBD. SBD colocalized to a large extent (~50%), mainly at the plasma membrane, with wild-type cdc42-GFP after 15 minutes (Fig. 2M,O). However, in cells expressing the dominant-negative form (cdc42-DN–GFP), the colocalization with SBD was dramatically reduced (Fig. 2N,O), as well as its uptake (see following section).

Dynamin is a large GTPase that mediates many forms of endocytosis and vesicle formation through its ability to tubulate and sever membranes (Praefcke and McMahon, 2004). Because dynamin-mediated uptake is thought to be functionally separate from the small GTPase-mediated mechanisms such as RhoA and cdc42 that internalize certain raft cargoes (Glebov et al., 2006; Mayor and Pagano, 2007; Payne et al., 2007; Sabharanjak et al., 2002), and because cdc42-DN only partially inhibited uptake (~35% inhibition; see below), we asked whether dynamin might be involved in a parallel uptake mechanism for SBD. In order to test the role of dynamin in the internalization of SBD, we used two approaches. First, SH-SY5Y cells were treated with Dynasore (Sigma), a cell-permeable drug that inhibits dynamin-1 and dynamin-2 (Macia et al., 2006). Dynasore treatment, as expected, almost completely blocked the uptake of the control Tfn-Alexa594 (Fig. 3A), whose clathrin-mediated internalization requires dynamin (Sever et al., 2000). To our surprise, Dynasore also inhibited internalization of SBD, the uptake being 46% that of untreated control cells (Fig. 3A,B).

As an alternative method to investigate the dynamin-dependence of SBD uptake, we transfected SH-SY5Y cells with a dynamin-2 dominant-negative mutated version, dynK44A DN (Damke et al., 2001) that suppresses the function of the endogenous dyanmin-2 protein. Whereas the amount of Tfn that entered cells transfected with dynamin-2 WT plasmid was not affected, the entry of Tfn in cells transfected with dynK44A DN was very low (Fig. 3B,C). Similarly, SBD internalization was reduced by more than half in cells transfected with dynK44A DN compared with cells transfected with dynamin-2 WT (Fig. 3B,C). We conclude that the internalization of SBD is not only mediated by cdc42 but also by dynamin.

To confirm that clathrin is not involved in the internalization of SBD, we tested the uptake of SBD in the presence of drugs that inhibit clathrin-mediated endocytosis. To inhibit clathrin-mediated endocytosis, SH-SY5Y cells were treated with 5 μg/ml chlorpromazine (CPZ) for 30 minutes prior to the addition of SBD. This treatment, as expected, completely blocked the endocytosis of Tfn (Fig. 3D,E), which requires clathrin-mediated endocytosis. In comparison, chlorpromazine did not inhibit the entry of SBD (Fig. 3D,E).

Neuronal cells, including SH-SY5Y, do not express caveolin (Gorodinsky and Harris, 1995). The efficient internalization of SBD by SH-SY5Y cells and other neurons (Steinert et al., 2008) implies that the uptake of SBD is independent of caveolin.

Flotillin and Rho family GTPases synergistically affect SBD internalization

As SBD showed colocalization with flotillin-2 after endocytosis (see Fig. 2), and because the internalization of both Aβ and the App precursor were shown to depend on flotillin as well as dynamin (Saavedra et al., 2007; Schneider et al., 2008), we next investigated the role of flotillin-2 in mediating SBD uptake and intracellular transport. We used siRNA to knock down the expression of flotillin-2 (see Materials and Methods), which we found reduced the amount of flotillin-2 expressed in cells to ~20% of normal (supplementary material Fig. S1) This was similar to the findings of other authors (Schneider et al., 2008). It was reported previously that loss of flotillin-2 also leads to proteasomal degradation of flotillin-1, reducing the possibility that loss of flotillin-2 could be masked by the remaining flotillin-1 (Langhorst et al., 2005; Solis et al., 2007). Knockdown of flotillin-2 reduced SBD uptake to ~69% of normal (Fig. 4A).

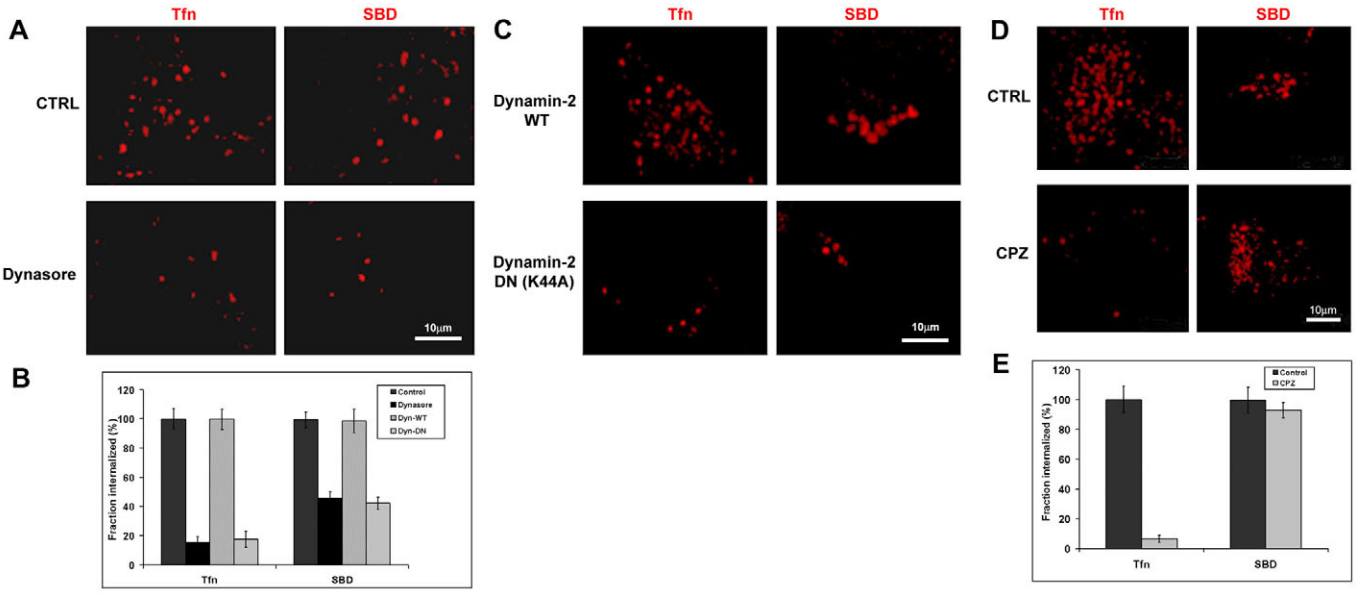

Fig. 3. SBD uptake is sensitive to dynamin inhibition, but not to inhibition of clathrin-mediated uptake. (A,B) Tfn-Alexa594 and SBD-TMR uptake after 60 minutes in control cells (CTRL; dark gray bars) compared with cells treated with Dynasore 80 μm for 30 minutes (black bars). (B,C) Tfn-Alexa594 and SBD-TMR in cells transfected with wild-type dynamin-2 (gray bars) compared with cells transfected with dynamin-2-DN (K44A) (light gray bars). (D,E) Tfn-Alexa594 and SBD-TMR uptake in cells treated with 5 μg/ml chlorpromazine (CPZ). Tfn uptake was strongly inhibited, whereas SBD uptake was normal. Values in B and E represent means ± s.e.m.

Clostridium toxin B was used to inhibit the activity of Rho family GTPases, including cdc42, which had already been implicated in toxin SBD uptake because of the inhibition by cdc42-DN–GFP. After treatment with clostridium toxin, SBD uptake was again inhibited, moderately, to ~74% of normal levels (Fig. 4A).

Inhibition of SBD uptake was determined by calculating the total internalized fluorescence per pixel within cells, excluding the plasma membrane, after imaging 60 minutes post-labeling (see Materials and Methods). When the two treatments were combined, flotillin-2 siRNA and inhibition with clostridium toxin together gave effects on SBD uptake that were much stronger than additive (reduction to 9% of normal) (Fig. 4A). Tfn uptake was, by contrast, unaffected by the combined treatment, indicating that the drastically reduced uptake of SBD was not simply due to cellular damage.

Because the foregoing method of assaying the amount of SBD taken up by the cells is restricted to quantification of SBD that has been internalized and is no longer associated with the plasma membrane, we decided to examine the effects of flotillin-2 siRNA and clostridium treatments on uptake and association of SBD by using fluorescence activated cell sorting (FACS). The results of this experiment paralleled those of the previous image analysis uptake assay, in that SBD appeared to be taken up less efficiently after either treatment alone, but that both treatments together had the most drastic effects (Fig. 4B). Using this assay we were able to assess association with the membrane, as opposed to uptake per se, by comparing total cell fluorescence pre- and post-washing. This is indicated by the difference between the red and the green traces, which show pre-washing and post-washing total fluorescence per cell, respectively (plotted in Fig. 4B).

By this measure, the amount of SBD loosely associated with the cells appeared to be reduced after either or both of the treatments, because the difference between pre- and post-washing was substantially smaller. Indeed, even the absolute levels of pre-washing fluorescence, as indicated by the red traces, were reduced by siRNA flotillin-2 and clostridium toxin, suggesting less initial association of SBD with the membrane. Uptake was also reduced by these treatments, shown by a decrease in absolute levels of post-washing fluorescence (green traces). After both treatments (last bar in lower graph, Fig. 4B), association with the membrane and uptake were both strongly abrogated, as both red and green traces pre- and post-washing were close to control (unlabeled) fluorescence levels. From these results, we conclude that the activity of either of these two molecules (flotillin-2 or a Rho GTPase) is required to allow some association and uptake of SBD at the membrane; however, both flotillin-based and Rho-GTPase-based mechanisms together synergize to effect efficient and complete SBD uptake.

Inhibition of either Rho GTPase or flotillin affects interaction of SBD with the cell surface and eradicates slow raft-like diffusion

Using fluorescence correlation spectroscopy (FCS), we tested the effects of blocking different mechanisms of SBD uptake on its diffusion behavior at the plasma membrane surface of neuroblastoma cells. Diffusion time of the fluorescent probe across a stationary confocal volume can be derived from the autocorrelation function $G(\tau)$ of fluorescent signals recorded from this volume over time. Different models that take into account one or more diffusing particles and two- or three-dimensional diffusion can be fitted to the $G(\tau)$ function. Because diffusion speed is a reflection of membrane fluidity, which is known to be decreased in raft domains (Bacia et al., 2004; Eggeling et al., 2008; Goswami et al., 2008; Pinaud et al., 2009), diffusion times (τ_D) from a confocal spot centered at the plasma membrane can be used to deduce membrane microdomain localization. This method was used previously to show that SBD displays a slow diffusion component at the plasma membrane, similarly to CtxB, but unlike uniformly distributed lipophilic dyes (Hebbar et al., 2008).

The fits to the correlation functions of fluorescent particles diffusing through the confocal volume are determined in multiple

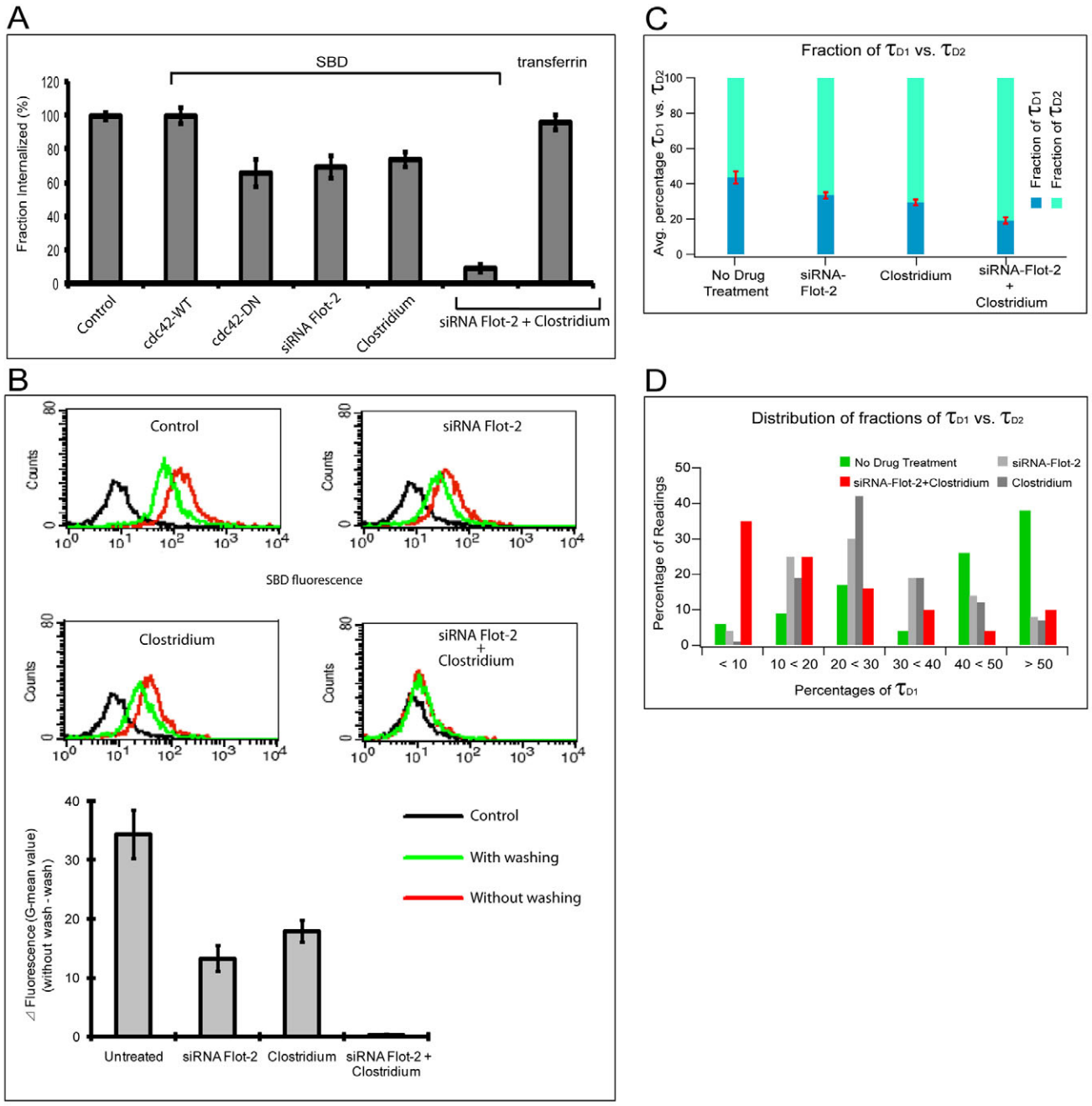

Fig. 4. Flotillin-2 and a Rho family GTPase act synergistically on SBD uptake, and both affect the proportion of SBD exhibiting slow diffusion (τ_{D1}). (A) Cdc42 inhibition by cdc42-DN, flotillin inhibition by flotillin-2 siRNA, and Rho GTPase inhibition by clostridium toxin B each reduced SBD uptake by ~65-75% of control. Simultaneous treatment with flotillin-2 siRNA and clostridium reduced uptake to only 9% of control, but did not affect transferrin uptake significantly. (B) FACS measurement of SBD-TMR fluorescence associated with cells showed reduced binding and uptake after treatment with flotillin-2 siRNA or clostridium toxin B. The graphs show histograms of cell counts (*y*-axis) with the given amount of fluorescence from SBD-TMR (*x*-axis). Black traces are unlabeled cells; green traces are labeled cells after washing; red traces are labeled cells before washing. Both traces shift to the left (lower fluorescence levels) after individual treatments, and shift to nearly control (unlabeled) levels after both treatments. The difference between fluorescence before and after washing (ΔFluorescence G-mean value; lower bar graph) also decreased upon either treatment, and dropped most drastically after both treatments. (C) Average proportions of FCS measurements fitting to τ_{D1} or τ_{D2} after interference with flotillin, Rho family GTPases, or both, show that the fraction of the faster diffusing component, τ_{D2} (light green), increased. (D) Histogram showing the distribution of FCS readings where the given proportion of τ_{D1} to τ_{D2} (given as percentage τ_{D1} on the *x*-axis) occurred. In control cells (green bars), most readings gave >40% τ_{D1}, whereas treatment with both flotillin-2 siRNA and clostridium (red bars) shifted the proportion of τ_{D1}in most measurements to <10%. Either treatment alone (gray bars) gave intermediate proportions of τ_{D1}. Values in A and B represent means ± s.e.m.

20-second cumulative measurements, and are generally separable into two components, fraction 1 and fraction 2 (Frn1 and Frn2), from which diffusion times can be derived. τ_{D1} (in the millisecond range) and τ_{D2} (in the microsecond range) are the slow and the fast components, respectively, and correspond to 2D-diffusing, membrane-bound label (τ_{D1}), and to 3D-diffusing, unbound label (τ_{D2}). By comparison with control $G(\tau)$ values of unbound label in solution (with an average τ_D in the microsecond range), it can be

inferred that τ_{D2} is mostly attributable to this unbound population (Wohland et al., 2001). It should be noted that FCS measurements inside the cell also give a predominantly τ_{D2} (microsecond) component, possibly due to internalized SBD that might diffuse through endosomes.

By comparing the proportion of particles that fall into the τ_{D1} or τ_{D2} categories (Frnτ_{D1} or Frnτ_{D2}) it is possible to determine whether the binding of SBD is affected under different treatments. Because the proportion of τ_{D1} and τ_{D2} will be affected if the confocal volume is not centered on the plasma membrane, care was taken to ensure that the confocal volume was always properly positioned at the plasma membrane. Frnτ_{D1} and Frnτ_{D2} were plotted in control, untreated cells and in cells treated with either flotillin-2 siRNA or clostridium toxin, or both (Fig. 4C). The fraction of τ_{D1} (the presumptive membrane-bound, millisecond range) fell from 44% in controls to 33% with flotillin-2 siRNA, 29% with clostridium treatment, and 19% with both treatments. Thus, the magnitude of the effect of knocking out either of the uptake mechanisms alone was similar, and removing both gave an almost perfectly additive effect on the binding of SBD. This implies that the effects of flotillin and cdc42 on the binding of SBD are additive, if one assumes that a decreased proportion of Frn1 reflects a loss of binding. This is in contrast to the effects on uptake, which we saw in the previous section were synergistic.

By plotting the percentage fraction of τ_{D1} in the different readings as a histogram instead of an average (Fig. 4D), it can be seen that the distribution of readings shifts from predominantly τ_{D1} (>50% putative membrane-bound particles) to smaller fractions of τ_{D1} (20-30%) under either siRNA treatment or treatment with clostridium toxin, and even smaller fractions (<10%) under both treatments simultaneously.

A previous study (Hebbar et al., 2008) that characterized the diffusion behavior of SBD on neuroblastoma cells showed that the diffusion rate of SBD averages ~50 milliseconds (also confirmed here; Fig. 5A) but, when plotted as a histogram, the diffusion rate distributes into two separate categories, one of ~1-10 milliseconds and the other of >30 milliseconds (see Fig. 5B). In that study, CtxB, but not the non-raft markers, also showed a bimodal distribution like that of SBD, and the slow component could be eliminated by methyl-β-cyclodextrin (mβCD). This suggested that the long diffusion time might correspond to the proportion of molecules that are associated (transiently) with a raft or nanocluster.

We now wanted to know whether the bimodal diffusion distribution was related to the different uptake mechanisms that affect SBD internalization into cells. Indeed, when treated with either clostridium toxin or flotillin-2 siRNA, or both, the slow component disappeared, being reflected in the much faster average τ_D (Fig. 5A) and in the shift of the histogram distribution to between 1-10 millisecond (Fig. 5B) under each of the three treatments.

In contrast to the τ_{D1} values, τ_{D2} values were not as strongly affected, although the average τ_{D2} sped up by about 50% (Fig. 5C), and the histogram of τ_{D2} did show a shift of τ_{D2} towards faster values under the combined flotillin-2-RNAi–clostridium treatment (but not either treatment alone) (Fig. 5D). This shift in τ_{D2} could be explained if τ_{D2} derives from freely diffusing SBD both outside the cell and inside the cell, because extracellular SBD has an average τ_D of ~115±5.8 microseconds (exclusively <200 microseconds; n=24 readings) whereas cytosolic τ_D averages 499.3±35.7 microseconds (exclusively >200 microseconds; n=45 readings) (supplementary material Fig. S2). Less efficient binding would also result in less SBD entering the cell, and therefore faster average τ_{D2} values.

In order to determine whether the decrease in τ_D values was a result of a general increase in membrane fluidity induced by the RNAi and clostridium treatments, we measured the τ_D values of a uniformly distributed lipophilic membrane dye, dialkylindocarbocyanine-C18 (DiI). The average values and histogram distribution of τ_D remained unchanged after individual and combined treatments (supplementary material Fig. S3).

The results above suggest that the combined effects of flotillin and Rho family GTPase on binding of SBD are stronger than either one alone and are additive; however, because removing either flotillin or Rho GTPases completely abolishes the slow diffusion

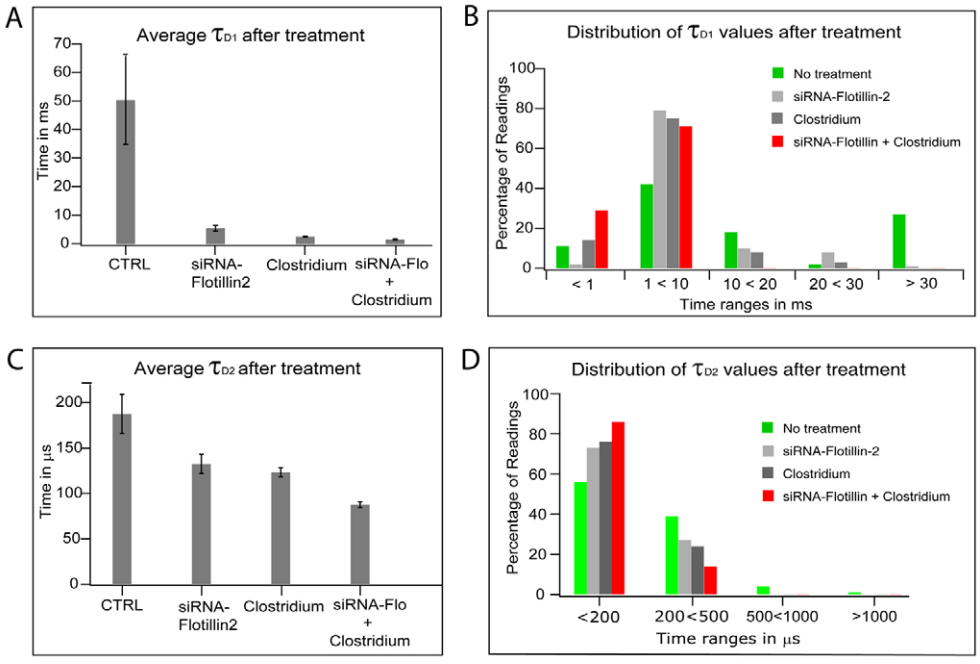

Fig. 5. Both flotillin and Rho family GTPase are required for the slow raft-like diffusion component of SBD. (A) Average τ_{D1} values (in milliseconds; *y*-axis) after interference with flotillin-2 or Rho family GTPases by clostridium toxin, or both. τ_{D1} values were as follows: control, 50.6±15.6 milliseconds; siRNA flotillin, 5.6±0.88 milliseconds; clostridium, 2.7±0.21 milliseconds; siRNA flotillin+clostridium, 2.0±0.27 milliseconds. (B) Histogram distribution of τ_{D1} values after the above treatments, showing disappearance of the slow (>30 milliseconds) component after either treatment alone (gray shades), or both together (red). (C) Average τ_{D2} values (in microseconds; *y*-axis) after above treatments. τ_{D2} is lower overall. τ_{D2} values were as follows: control, 187.5±21.2 microseconds; siRNA flotillin, 132.4±8.7 microseconds; clostridium, 123.3±4.9 microseconds; siRNA flotillin+clostridium, 93.7±4.5 microseconds. Histogram distribution of τ_{D2} values after above treatments. After both treatments together, a higher percentage of readings gave τ_{D2} values of <100 microseconds (red). Values in A and C represent means ± s.e.m.

component of SBD, both of these mechanisms must be absolutely required for this raft-like diffusion behavior.

SBD intracellular trafficking pathway is determined by cdc42- and flotillin-mediated uptake

To test the involvement of Rho family GTPases and flotillin in regulating SBD intracellular targeting, colocalization studies were carried out with SBD and intracellular markers after interference with these pathways, using the same methods as above. First, flotillin-2–GFP localization was confirmed in SH-SY5Y neuroblastomas to localize ~50% to an endolysosomal compartment identified by lysotracker red (supplementary material Fig. S4), in agreement with earlier studies (Langhorst et al., 2008). In control cells, SBD efficiently targeted early endosomes at 30 minutes after endocytosis, where it colocalized to ~50% with early endosomal antigen 1 (EEA1) and this was unaffected by interference with clathrin-mediated uptake using chlorpromazine (Fig. 6A,B). siRNA knockdown of flotillin-2 significantly reduced the degree of colocalization of SBD with EEA1 (Fig. 6C,F), indicating that flotillin internalization is a prerequisite for further delivery of SBD to an early endosomal sorting compartment.

Next, we tested the role of flotillin-2 in mediating SBD trafficking to recycling endosomes and lysosomes, respectively. In control cells, SBD localized ~50% in rab11-GFP-positive recycling endosomes, and ~45% in acidic lysotracker-positive lysosomes after 1 hour (Fig. 6D-F). This late association with recycling endosomes is in accordance with earlier characterization in another cell type (Steinert et al., 2008), showing that SBD takes a slow route through sorting endosomes before it reaches recycling and degradative compartments.

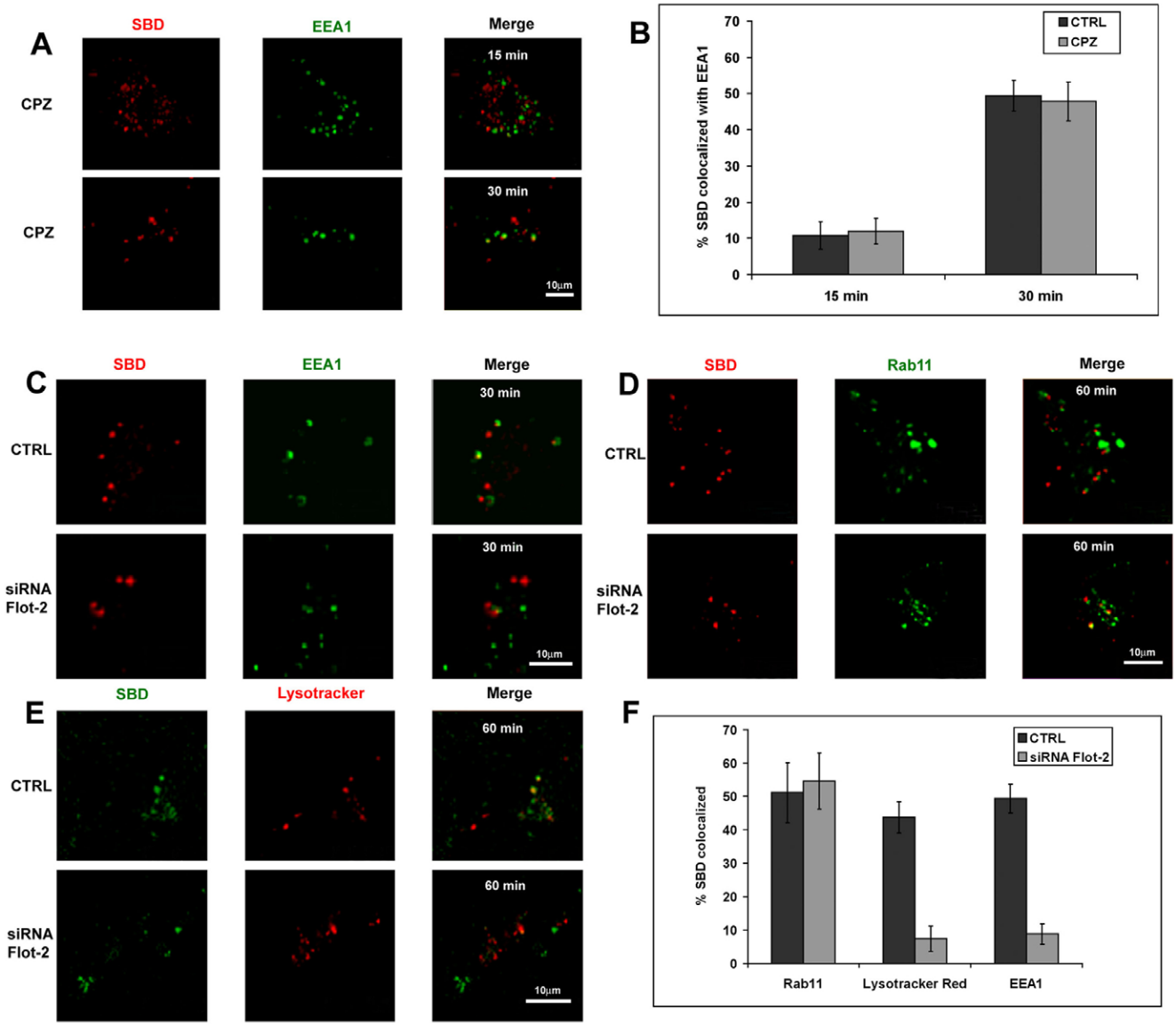

Fig. 6. SBD is directed into a degradative pathway by flotillin-mediated uptake. (A,B) SBD (red) is taken partially into an EEA1-positive (green) early endosomal compartment after 30 minutes, and this is unaffected by chlorpromazine (CPZ) inhibition of clathrin uptake. (C,F) SBD (red) uptake into EEA1-containing early endosomes (green) is inhibited by interference with flotillin-2. (D,F) SBD (red) trafficking to rab11-GFP-positive recycling endosomes (green) is unaffected by interference with flotillin-2. (E,F) SBD (green) trafficking to lysotracker-red-positive degradative compartments is inhibited by interference with flotillin-2. Values in B and F represent means ± s.e.m.

Notably, knocking down expression of flotillin-2 did not affect the targeting of SBD to rab11-positive recycling endosomes at all, in spite of its effect on EEA1 (Fig. 6D,F; above). By contrast, and similarly to its effect on early endosomes, flotillin-2 siRNA strongly decreased the amount of SBD trafficking to lysosomes (Fig. 6E,F).

We next sought to identify the intracellular trafficking pathways regulated by cdc42-mediated uptake of SBD, because we found in the previous experiments that uptake is mediated by a combination of flotillin and a Rho GTPase, most likely cdc42. Using clostridium B toxin to inhibit the activity of cdc42 (along with other Rho family GTPases), we found that the transport of SBD to recycling endosomes was largely blocked (Fig. 7A,C). However, SBD trafficked normally to lysosomes at 1 hour after endocytosis in spite of the inhibition of Rho GTPases (Fig. 7B,C). Together, these data show that inactivation of Rho GTPases inhibits the SBD trafficking to recycling endosomes, but not to lysosomes. Conversely, knockout of flotillin-mediated uptake inhibits SBD trafficking to lysosomes, leaving the recycling pathway unaffected.

Cholesterol regulates SBD trafficking pathways

As described in the previous section for inhibitors of uptake, we asked whether cholesterol was involved in intracellular trafficking of SBD in SH-SY5Y neuroblastomas. We had earlier determined that cholesterol was required for uptake in both mammalian and insect cells (Hebbar et al., 2008) and that sterol content modulated the trafficking of SBD to a degradative pathway in insect cells (Steinert et al., 2008). We first depleted cells of cholesterol using mβCD and observed cholesterol removal by staining the cells with filipin, a fluorescent polyene antibiotic (Beknke et al., 1984). High concentrations of mβCD (10 mM) were seen previously to result in effective depletion of cholesterol (50% reduction) from SH-SY5Y cells and subsequently blocked the uptake of SBD (Hebbar et al., 2008). Similar results were seen here (supplementary material Fig. S5), but we found that the uptake of SBD was not eradicated by milder cholesterol depletion using only 2 mM mβCD (although at this concentration, the diffusion speed at the membrane is affected; M.M., T.W. and R.K., unpublished results). Using this treatment, we were therefore able to assess the effect of cholesterol depletion on SBD trafficking. SBD trafficking to recycling endosomes was inhibited by mild cholesterol depletion (Fig. 8A,B) to a similar extent as with cdc42 inhibition (i.e. from ~50% to ~20%; see Fig. 7). Repletion of cholesterol to the membrane with mβCD-cholesterol complexes restored trafficking to the recycling compartment (Fig. 8A,B). Cholesterol depletion also substantially inhibited trafficking of SBD to lysosomes, and this could again be restored by cholesterol repletion (Fig. 8C,D).

We next wanted to determine the effect of cholesterol in the endolysosomal system on SBD trafficking. To induce intracellular cholesterol storage, we used U18666A, a drug known to lead to accumulation of cholesterol in lysosomes, similar to the accumulation seen in Niemann-Pick type C and the lipid storage diseases (Roff et al., 1991). In U18666A-treated SH-SY5Y cells, cholesterol accumulated in enlarged lysosomes, as expected (supplementary material Fig. S4). In U18666A-treated cells, we observed that this disrupted cholesterol distribution resulted in markedly more SBD accumulation in lysosomes than in controls (Fig. 8D) compared to untreated cells ($P<0.01$). Depletion of cholesterol from U18666A-treated cells with mβCD in turn reduced

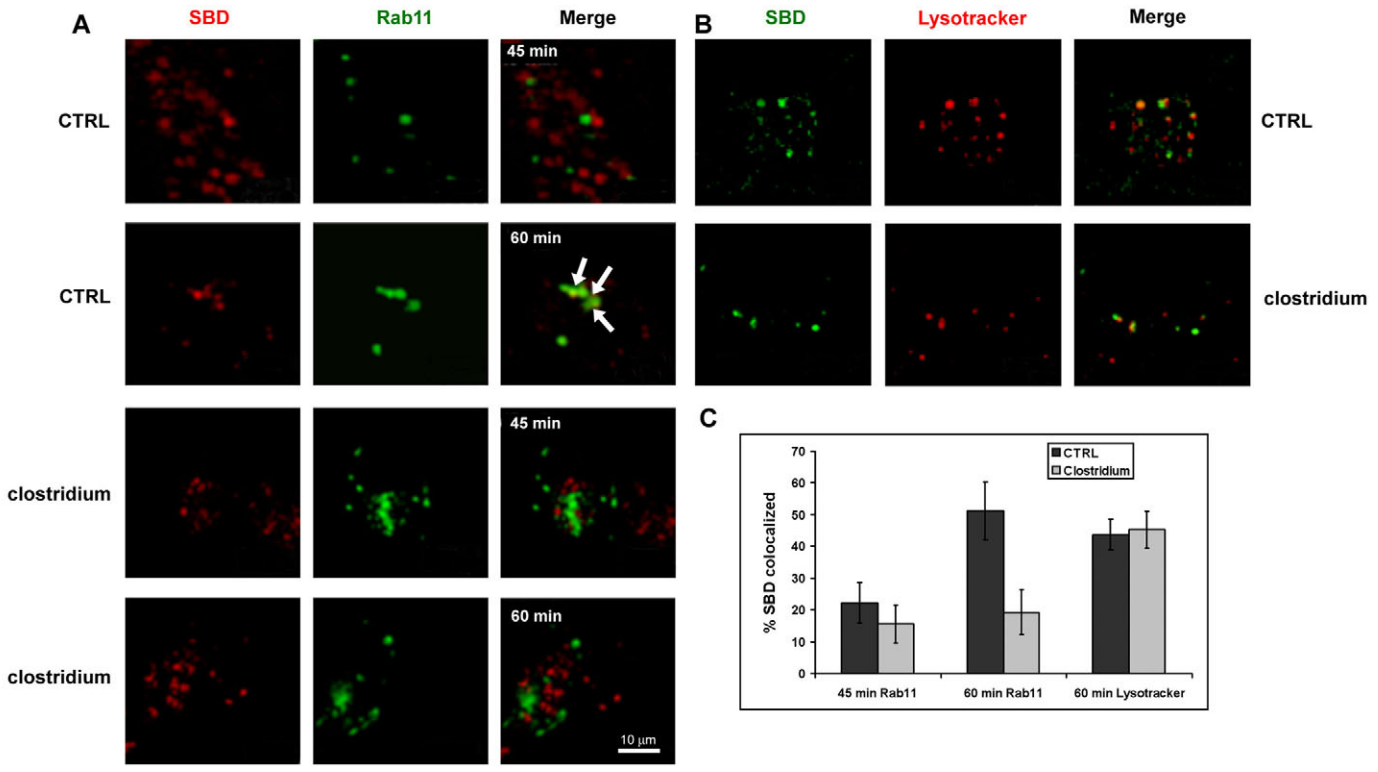

Fig. 7. SBD is directed into a recycling pathway by a Rho family GTPase. (A,C) SBD (red) colocalizes increasingly between 45 and 60 minutes with rab11-GFP-positive recycling endosomes in control cells (top), and this is reduced after inhibition of Rho family GTPases (bottom) with clostridium toxin. (B,C) SBD (green) colocalization with lysotracker-positive compartments is unaffected by treatment with clostridium toxin. Values in C represent means ± s.e.m.

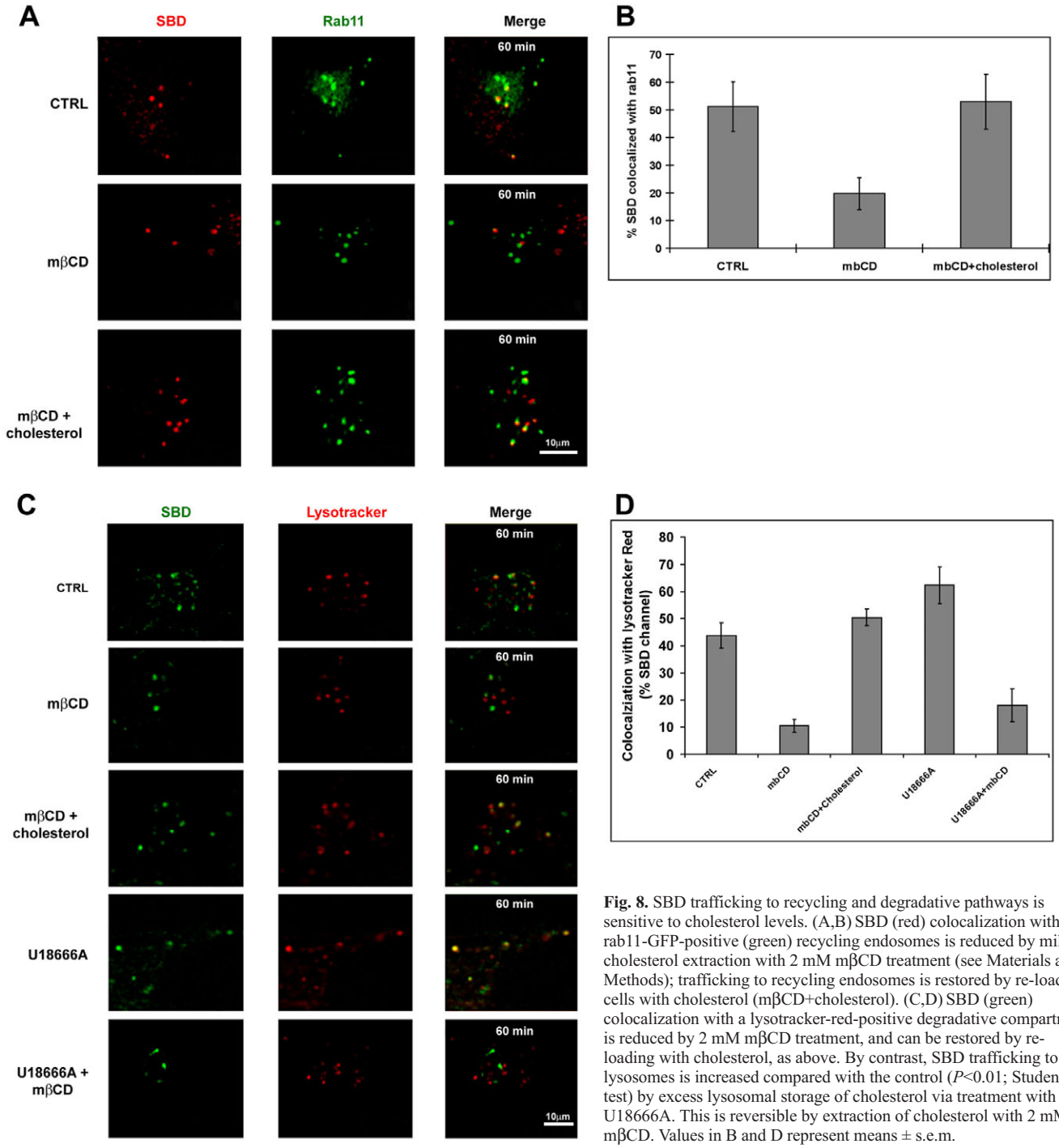

Fig. 8. SBD trafficking to recycling and degradative pathways is sensitive to cholesterol levels. (A,B) SBD (red) colocalization with rab11-GFP-positive (green) recycling endosomes is reduced by mild cholesterol extraction with 2 mM mβCD treatment (see Materials and Methods); trafficking to recycling endosomes is restored by re-loading cells with cholesterol (mβCD+cholesterol). (C,D) SBD (green) colocalization with a lysotracker-red-positive degradative compartment is reduced by 2 mM mβCD treatment, and can be restored by re-loading with cholesterol, as above. By contrast, SBD trafficking to lysosomes is increased compared with the control ($P<0.01$; Student's *t*-test) by excess lysosomal storage of cholesterol via treatment with U18666A. This is reversible by extraction of cholesterol with 2 mM mβCD. Values in B and D represent means ± s.e.m.

colocalization of SBD with lysosomes to lower than normal levels (Fig. 8C,D). Taken together, these results suggest that the intracellular trafficking behavior of SBD is sensitive to cholesterol content in both the early and late parts of the pathway.

Discussion

The uptake mechanisms and intracellular trafficking of SBD, a fluorescently tagged sphingolipid interacting peptide probe, were examined in a human neuroblastoma line, SH-SY5Y. Unlike other microdomain-associated cargoes that have been characterized thus far, SBD was found to be endocytosed approximately equally by a cdc42-mediated pathway, and by a second pathway involving the lipid-raft-associated adaptor protein, flotillin (Langhorst et al., 2005; Mayor and Pagano, 2007). cdc42 has been implicated in regulating the GEEC pathway, specific for the uptake of GPI-linked proteins (Sabharanjak et al., 2002), which in some cases can also be endocytosed by flotillin-mediated mechanisms, although this is disputed (Glebov et al., 2006; Langhorst et al., 2008). Accordingly, SBD colocalized extensively in endosomes containing cdc42-GFP, flotillin-2–GFP and GPI-AP–GFP, although it segregated almost completely from another raft- and sphingolipid-interacting marker, CtxB.

SBD uptake by cdc42- and flotillin-mediated mechanisms is synergistic

Because SBD uptake is strongly affected by dynamin interference, and because knockout of Rho-GTPases (which include cdc42) and flotillin together virtually eliminates SBD uptake, we have to assume that dynamin takes part in one or other of the uptake mechanisms (i.e. cdc42 and/or flotillin), and does not constitute part of a third independent mechanism. According to the studies of Mayor and colleagues (Chadda et al., 2007; Sabharanjak et al., 2002) with GPI-APs, the cdc42 pathway is non-overlapping with dynamin mechanisms. However, a scenario combining the two would not be unprecedented because interleukin 2 receptor (IL2-R) endocytosis, which is also not clathrin-mediated, is simultaneously dynamin- and Rho-dependent (Lamaze et al., 2001). Furthermore, uptake that is jointly mediated by dynamin and flotillin has been documented multiple times. For example, and particularly relevant for this study, Schneider et al. reported that flotillin is involved in the uptake and clustering of App, even though App also requires dynamin and clathrin-adaptor proteins (Schneider et al., 2008). Uptake of Aβ (the parent molecule of SBD) is also dynamin-dependent (Saavedra et al., 2007). Zhuang and colleagues also describe a dynamin- and flotillin-mediated mechanism (Payne et al., 2007) responsible for the uptake of cationic agents like polyethylenimine (PEI) and Lipofectamine, but this was unaffected by cholesterol depletion.

In this study, we used three different methods to assay the effects of interference with flotillin- and Rho-GTPase-mediated pathways on SBD binding and uptake. First, quantification of internalized SBD by standard fluorescence imaging showed that removing either the flotillin pathway or the Rho-GTPase pathway by treatment with clostridium toxin exerted moderate effects on SBD uptake, whereas knockout of both mechanisms together nearly eliminated uptake. FACS quantification indicated that this reduced uptake was associated with reduced cell-surface-bound (i.e. washable) SBD after either treatment, and with stronger loss of cell-surface binding after both treatments. Accordingly, the FCS experiments also showed that an increased fraction of SBD diffused at the fastest rate, indicative of less binding, but these effects appeared to be additive for each treatment. Because the effects on actual uptake are probably synergistic, not additive, the results argue for involvement of both mechanisms in a single or strongly interacting internalization process.

The notion of a single, highly efficient uptake process dependent on both flotillin and cdc42 simultaneously is also supported by our observation that knockout of either mechanism alone completely abolishes the slowest diffusion component (see below). Synergism between two mechanisms might also explain the situation noted by Glebov and colleagues (Glebov et al., 2006), in which simultaneous DynK44A DN and flotillin-siRNA knocked out CtxB uptake by 80%, even though the effect of DynK44A DN alone was much less severe, and flotillin-siRNA alone had no significant effect. Thus, on the same principle by which geneticists predict protein interactions based on synergistic interactions between different mutations, we predict that there might be a direct interaction between flotillins and cdc42.

Slow plasma membrane diffusion is associated with a combinatorial uptake mechanism

In a previous study using FCS, we showed that diffusion of SBD at the plasma membrane distributed into two categories: those with medium τ_D values (~1-10 milliseconds) and those with slow τ_D values (~50 milliseconds), whereas the non-raft-associated lipid analogs DiI and 4,4-difluoro-4-bora-3a,4a-diaza-*s*-indacene (BODIPY)-Sphingomyelin diffused only in the medium (1-10 milliseconds) range. Interestingly, CtxB in that study showed a very similar bimodal distribution,

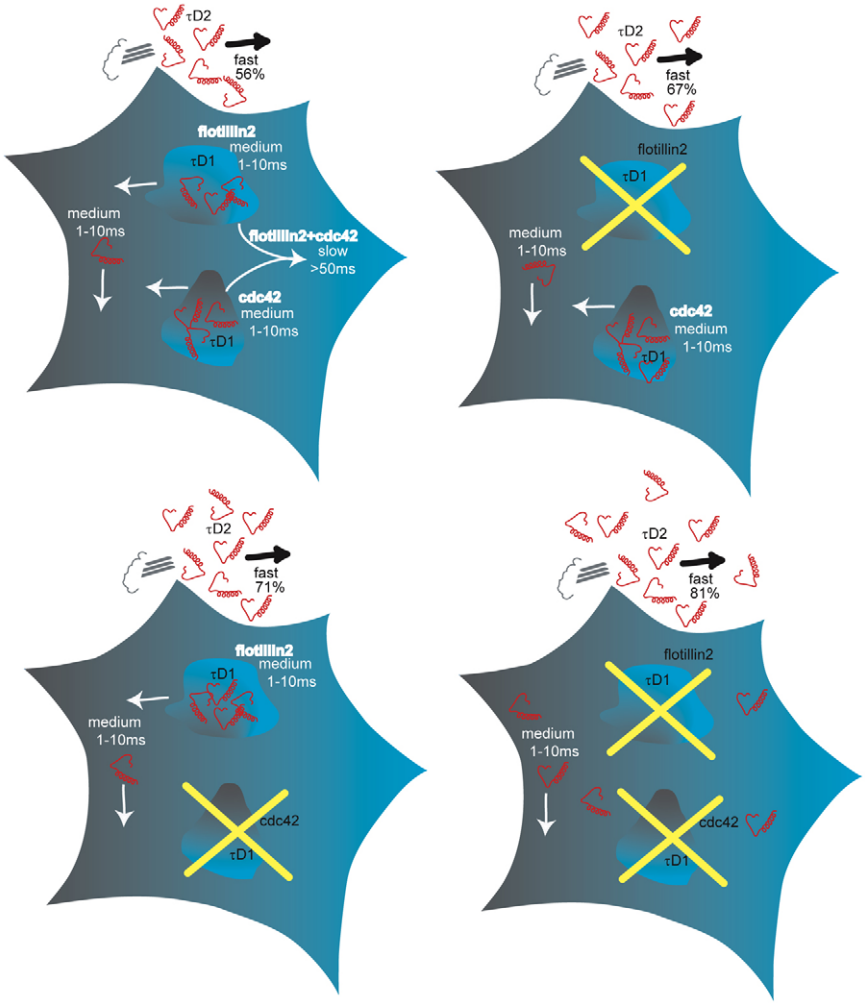

Fig. 9. Model showing proposed origin of the slow-, medium- and fast-diffusing SBD components. In the model, τ_{D2} represents the fast (microsecond range), unbound population of SBD that is presumably outside the cell (56%), but still registered by FCS measurement. Both flotillin and cdc42 associated mechanisms alone can mediate suboptimal uptake and medium-speed diffusion (1–10 milliseconds). Flotillin and cdc42 together synergistically mediate slow (>50 milliseconds) diffusion and efficient uptake. When either or both flotillin- or cdc42-mediated uptake mechanisms are knocked out, the fast unbound population of SBD increases to 67%, 71% or 81%, respectively, and the very slow (50 milliseconds) diffusion component is removed. A small proportion of SBD associated with neither mechanism remains at the surface and diffuses at a medium speed (1–10 milliseconds).

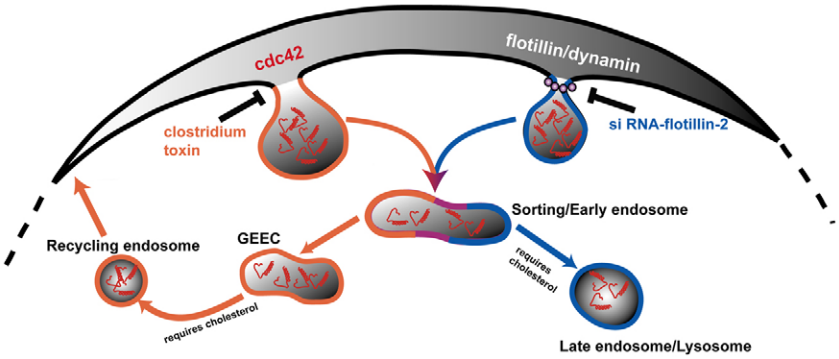

Fig. 10. Schematic summary of uptake mechanisms and subsequent trafficking routes of SBD. Under normal cholesterol conditions, SBD is taken up by a mechanism that requires both cdc42 and flotillin. SBD can also be internalized by either cdc42- or flotillin-mediated uptake alone, but this leads to different intracellular targeting – exclusively recycling in the case of cdc42, and exclusive degradation in the case of flotillin. The model does not exclude the possibility that flotillin and cdc42 could act synergistically at the membrane.

as did another presumptive raft-localizing sterol lipid analog [M.M., T.W., Gary Jennings (JADO Technologies, GmbH, Dresden, Germany) and R.K., unpublished results]. Suggestively, the longer diffusion time could be eliminated by mβCD and sphingolipid depletion (Hebbar et al., 2008) (M.M., T.W. and R.K., unpublished results) (see also Lasserre et al., 2008), indicating that the slowly diffusing fraction might correspond to the proportion of molecules that are associated (transiently) with a raft or nanocluster (Sharma et al., 2004). Here, we wondered whether this apparently raft-diagnostic long diffusion time corresponded to uptake by cdc42- and/or flotillin-mediated mechanisms. Surprisingly, whereas neither of these mechanisms was absolutely required to achieve some uptake (see previous section), the slow diffusion component was completely abolished when either mechanism was knocked out. This suggested that the slow diffusion might in fact correspond to a highly efficient, cdc42+flotillin synergistic uptake mode. A model proposing a link between diffusion behavior and uptake mode is shown in Fig. 9. A number of approaches could be used to test this model, including colocalization by super-resolution fluorescence imaging methods, or fluorescence cross-correlation spectroscopy, in parallel with studies of uptake kinetics.

Similar bimodal diffusion behaviors to that displayed by SBD have been seen before, notably in a recent study by Pinaud et al. (Pinaud et al., 2009), and earlier by Lommerse and colleagues (Lommerse et al., 2006). Other authors have recently derived diffusion constants from anisotropy and fluorescence recovery after photobleaching (ARAP and FRAP) (Goswami et al., 2008) and high-speed single-particle tracking (Umemura et al., 2008) on raft- and non-raft molecules; however, these either showed complete immobility associated with nanoclusters, or uniformly distributed hop-diffusion behaviors, irrespective of raft or non-raft localization. By contrast, Lassere and colleagues did find slow diffusion of raft-linked molecules (Lasserre et al., 2008). Unlike the present study, however, the diffusion behaviors in these studies were not linked to a particular uptake mechanism per se, but rather to cytoskeletal organization and raft lipid content.

Uptake mechanism influences the trafficking route

An important finding of this study was that the normally occurring combination of endocytic mechanisms, involving both cdc42 and flotillin, not only affected diffusion speed and efficiency of internalization, but also the subsequent trafficking route. After internalization, SBD is split roughly equally between recycling endosomes and lysosomes. Surprisingly, the balance between these two pathways appears to be strongly affected by the uptake mechanism. Targeting to recycling endosomes requires the activity of cdc42 (possibly implicating GEECs in this recycling pathway) because GEECs target mainly to recycling endosomes and this is mediated by cdc42 (Chadda et al., 2007). Moreover, SBD, like GEEC-associated cargoes, has a very low degree of colocalization with Tfn (Sabharanjak et al., 2002). By contrast, targeting through the degradative pathway had a strong requirement for flotillin. This switch might reflect a connection of the uptake machinery (i.e. flotillin) with the requirement for a degradative rather than biosynthetic pathway for sphingolipids, perhaps in association with cholesterol and sphingolipid content at the plasma membrane. Support for this view (summarized in Fig. 10) was given by cholesterol overload and depletion experiments (below).

Membrane cholesterol content influences trafficking route

Interestingly, we found that cholesterol as well as the uptake mechanism is involved in the regulation of the SBD intracellular pathway. Moderate depletion of cholesterol reduced trafficking of SBD to recycling endosomes as well as to endolysosomes. The suppressive effect of mβCD cholesterol depletion on SBD recycling might, however, be brought about indirectly because cdc42 activity and exchange at the membrane are sensitive to cholesterol levels (Chadda et al., 2007). By contrast, overloading the lysosomal pathway with cholesterol left recycling unaffected, but measurably increased the amount of SBD found in degradative compartments.

These results are consistent with the idea that SBD recognizes sphingolipid- and cholesterol-rich regions of the membrane, and might be following their pathway to degradation under conditions of excess cholesterol storage. In this scenario, high cholesterol conditions would induce the degradation of sphingolipid and/or cholesterol pools or their recycling back to the surface, rather than further metabolic processing and storage. Cholesterol depletion, by contrast, might shunt sphingolipids away from both the degradative and recycling pathways, because under low cholesterol availability, more lipid should be stored and/or processed, rather than cycled out or degraded.

We propose that the behavior of SBD trafficking might reflect the function of its parent molecule Aβ, albeit without the physiological consequences of Aβ administration. As such, SBD accumulation in certain cellular compartments could serve as a metabolic ‘stop storing fat’ indicator, steered to these locations by the presence of high levels of sphingolipids and/or cholesterol (i.e. raft components), with the aid of accompanying endocytic accessory proteins such as cdc42 and flotillin.

Materials and Methods

Cell culture, transfection and drug treatments

SH-SY5Y neuroblastoma (ATCC, Manassas, VA) were cultivated at 37°C in Dulbecco’s modified Eagle’s medium (DMEM; Gibco) /F12 (1:1) supplemented with 10% fetal bovine serum (FBS; Gibco) and 1% antibiotic. The rat-flotillin-2–GFP

cDNA was kindly provided by Sean Sweeney and subcloned into a mammalian expression vector pcDNA3.1 (Invitrogen) as described previously (Hebbar et al., 2008). GFP–Cdc42-WT and GFP–cdc42-DN were kind gifts of Sohail Ahmed. Plasmid DNA (1 μg) was used along with Lipofectamine 2000 (Invitrogen) for transient transfections according to manufacturer's instructions. Experiments were carried out approximately 48 hours following transfection.

mβCD, cholesterol, HEPES, PMSF, Chlorpromazine, and Dynasore were obtained from Sigma (St Louis, MO). Cholesterol depletion and overload was carried out as previously described (Hebbar et al., 2008; Steinert et al., 2008). Chlorpromazine (5 μg/ml) was used to inhibit clathrin-dependent endocytosis by pretreating for 30 minutes at 37°C before cell labeling. For inhibition of dynamin activity, 80 μM Dynasore was incubated with cells in serum-free medium at 37°C for 30 minutes prior to subsequent experiments. To inhibit Rho family GTPase activity, including cdc42, cells were incubated with *Clostridium difficile* toxin B (40 ng/ml; Calbiochem) at 37°C for 1 hour.

SiRNA treatment

Cells were grown in eight-well chambers with 0.17 mm coverslip bottoms (Nunc, Denmark) one day before transfection. For transfection, 1 μl of Lipofectamine-2000 (Invitrogen) was diluted to 25 μl Opti-MEM I (Invitrogen), and the solution incubated for 5 minutes at room temperature. This mixture was then added to a second solution of siRNA (20 μM) in 25 μl Opti-MEM I and allowed to complex for 20 minutes at room temperature. After incubation, 150 μl of full growth medium without antibiotics was added to the Lipofectamine-2000–siRNA solution, and the resulting 200 μl was added to the cells. On day 2, cells were transfected with siRNA again according to the above procedure. In this second round of transfection with siRNA, cells were co-transfected with a GFP-tagged plasmid for use as a marker. At 48 hours after this co-transfection, cells were used for further experiments. A scrambled, non-specific siRNA construct was used as a control, and siRNA with the sequence 5′-UAACCUCCUCACUGAAGGdTdT-3′ was used against flotillin-2 (both from 1st BASE, Singapore).

Cell labeling

Cells were seeded at a density of 10^6 cells/ml into eight-well chambers with 0.17 mm coverslip bottoms (Nunc, Denmark). Experiments were conducted 24-72 hours post-seeding. Lysotracker staining of acidic compartments was done by incubating cells for 2 hours at 37°C with 75 nM lysotracker red (Invitrogen) in normal growth medium.

For labeling of free cholesterol with filipin, cells were fixed in 4% paraformaldehyde (PFA) for 20 minutes followed by washes in HBSS-HEPES. Cells were incubated with 50 μg/ml filipin (Sigma) for 30 minutes and then washed before imaging.

CtxB labelings were done with Vybrant Alexa594 (Invitrogen). Cells were incubated with 10 μg/ml CtxB in full growth medium. CtxB labeling was carried out without antibody cross-linking. Alexa-Fluor 594 Tfn (5 μg/ml; Molecular Probes) was added to cells in serum-free medium. For endocytic tracing experiments, cells were incubated with fluorescently labeled endocytic markers on ice for 15 minutes then washed to remove excess dyes before warming for the indicated times, and imaging. Double labelings with CtxB (Vybrant) or Tfn-Alexa and SBD were done by first incubating CtxB or Tfn for 10 minutes on ice, then washing quickly, and incubating with SBD (10 μM) for 15 minutes on ice, then washing and immediately imaging at 37°C.

Labelings for FCS experiments were carried out at a concentration of 10 nM for DiI and 30-50 nM for SBD.

Immunofluorescence

Cells were fixed with 4% PFA for 20 minutes at room temperature and then blocked (2% BSA, 0.5% Triton-X-100 in PBS) for 15 minutes at room temperature. The primary antibody (1 mg/ml) was added to the cells at a 1:200 dilution and incubated for 1 hour at room temperature. Alexa488- or Alexa568-coupled secondary antibody (Invitrogen; 1 mg/ml) was added to the cells (1:1000 in 0.2% BSA, 0.05% Triton-X100 in PBS) for 30 minutes. Cells were washed three times with 0.2% BSA and 0.05% Triton-X-100 in PBS between each step. Anti-EEA1 and anti-flotillin-2 monoclonal antibodies were purchased from BD Biosciences.

Imaging and image processing

For uptake experiments, images were acquired with a CoolsnapHQ CCD camera on a Deltavision (Applied Precision) inverted fluorescence microscope with a 60× 1.42NA oil lens (Olympus) and a standard (green ex490/20, em528/38; red ex555/28, em617/73) filter set (Chroma). Quantification of images was performed using MetaMorph. Internalized fluorescence was determined by drawing borders around individual cells and subtracting non-cellular background. Uptake was calculated as a percentage of control in non-treated cells after 60 minutes of post-labeling chase (fluorescence units per pixel in treated cells divided by fluorescence units per pixel in untreated cells, times 100). All photomicrographs in a given experiment were exposed and processed identically for a given fluorophore. The Costes thresholded colocalization algorithm was performed using ImageJ (rsb.info.nih.gov/ij) plugins 'Colocalization Test' and 'Colocalization Threshold' by T. Collins and W. Rasband, and 'BG Subtraction from ROI' by M. Cammer and T. Collins (www.uhnresearch.ca/facilities/wcif/imagej). Colocalization was carried out as previously described (Steinert et al., 2008) and the thresholded Manders coefficient (tM) was given as a percent to express the degree of colocalization of the SBD channel with the other channel. Each data point consisted of two separate experiments, taking into account at least ten cells each.

Flow cytometry analysis

SBD-TMR association with the plasma membrane and uptake by neuroblastoma SH-SY5Y cells was assayed by measuring the amount of SBD fluorescence associated with the cells by FACS measurement before and after washing. Briefly, untreated cells, or cells treated with clostridium toxin B or siRNA flotillin-2, or both, were labeled with SBD, as previously. SBD endocytosis was terminated by placing the cells on ice. The cells were immediately analyzed using a FACS BD flow cytometer in FL-2 channel without further washing. Alternatively, cells were extensively washed with cold PBS to deplete surface-bound SBD and then were analyzed using a flow cytometer in FL-2 channel. About 10,000 cells were analyzed for each sample in triplicate for each condition. The G-mean fluorescence intensity (GMFI) of the cells for each treatment was analyzed and compared with a negative control (unlabeled SH-SY5Y cells). The GMFI values of cells without washing derived from internalized SBD plus plasma-membrane-bound SBD. The GMFI values of cells with extensive washing were presumed to have derived only from internalized SBD. The plasma-membrane-associated SBD for each treatment was calculated by the difference in fluorescence (GMFI without wash minus GMFI with wash).

FCS measurement

FCS was carried out on an Olympus FV300 confocal microscope, equipped with 488 nm Argon and 543 nm He-Ne lasers, and in-house coupled correlator and Avalanche photodiode. Laser power was set to 100 μW before the objective. Cells were first imaged in transmitted light mode to find the *Z*-plane of the plasma membrane, and then FCS was performed in the point-scanning mode. The autocorrelation function $G(\tau)$ is calculated by the hardware correlator as $\{[\delta F(t)\,\delta F(t+\tau)]/[F(t)]^2\}$, where $F(t)$ is the fluorescence fluctuation caused by a particle entering the confocal volume and $F(t+\tau)$ by the same particle at time $(t+\tau)$ (Haustein and Schwille, 2003). IgorPro software was used to fit the data to 2D or 3D and one-particle (2D1P1t or 3D1P1t) or two-particle (2D2P1t or 3D2P1t), one-triplet models as follows:

2D1P1t:

$$G(\tau)=\frac{1}{N}\times\left[\left\{\frac{1}{(1+\tau/\tau_D)}\right\}\left\{1+\frac{F_{trip}}{(1-F_{trip})}\times e^{-(\tau/\tau_{trip})}\right\}\right]+1$$

2D2P1t:

$$G(\tau)=\frac{1}{N}\left[\left\{\frac{(1-F_2)}{(1+\tau/\tau_D)}\right\}\left\{\frac{F_2}{(1+\tau/\tau_{D2})}\right\}\left\{1+\frac{F_{trip}}{(1-F_{trip})}\times e^{-(\tau/\tau_{trip})}\right\}\right]+1$$

3D1P1t:

$$G(\tau)=\frac{1}{N}\left[\left\{\frac{(1+\tau/\tau_D)^{-1}}{\sqrt{1+(\tau/\tau_D)K^{-2}}}\right\}\left\{1+\frac{F_{trip}}{(1-F_{trip})}\times e^{-(\tau/\tau_{trip})}\right\}\right]+1$$

3D2P1t:

$$G(\tau)=\frac{1}{N}\left[\left\{\frac{(1-F_2)(1+\tau/\tau_D)^{-1}}{\sqrt{1+(\tau/\tau_D)K^{-2}}}\right\}\left\{\frac{F_2\times(1+\tau/\tau_{D2})^{-1}}{\sqrt{1+(\tau/\tau_{D2})K^{-2}}}\right\}\left\{1+\frac{F_{trip}}{(1-F_{trip})}\times e^{-(\tau/\tau_{trip})}\right\}\right]+1$$

where N is the number of particles in the observation volume, F_{trip} is the fraction of particles in the triplet state, t_{trip} is the triplet relaxation time, F_2 is the fraction of particles with correlation time t_2 (and 1-F_2, is then the fraction of particles with correlation time t_1), and K is the structure factor describing the ratio of the length of the observation volume to its width.

We are very grateful to Sohail Ahmed (Institute of Medical Biology, A-STAR, Singapore) for sharing cdc42GFP fusion constructs, and Sean

Sweeney and Laura Briggs (University of York, York, UK) for the flotillin-2–GFP plasmid. We thank Frederic Bard (Institute of Molecular and Cell Biology, A-STAR, Singapore) for donating plasmid constructs and Sean Liour for helpful discussions. Funding for this project was provided by the Institute of Bioengineering and Nanotechnology (Biomedical Research Council, Agency for Science, Technology and Research, Singapore), and the Singapore Bioimaging Consortium (SBIC grant #003/2005:R143-000-284-305). M.M. is a recipient of a National University of Singapore graduate scholarship.

References

Abrami, L., Liu, S., Cosson, P., Leppla, S. H. and van der Goot, F. G. (2003). Anthrax toxin triggers endocytosis of its receptor via a lipid raft-mediated clathrin-dependent process. *J. Cell Biol.* **160**, 321-328.

Bacia, K., Scherfeld, D., Kahya, N. and Schwille, P. (2004). Fluorescence correlation spectroscopy relates rafts in model and native membranes. *Biophys. J.* **87**, 1034-1043.

Beknke, O., Tranum-Jensen, J. and van Deurs, B. (1984). Filipin as a cholesterol probe. I. Morphology of filipin-cholesterol interaction in lipid model systems. *Eur. J. Cell Biol.* **35**, 189-199.

Chadda, R., Howes, M. T., Plowman, S. J., Hancock, J. F., Parton, R. G. and Mayor, S. (2007). Cholesterol-sensitive Cdc42 activation regulates actin polymerization for endocytosis via the GEEC pathway. *Traffic* **8**, 702-717.

Damke, H., Binns, D. D., Ueda, H., Schmid, S. L. and Baba, T. (2001). Dynamin GTPase domain mutants block endocytic vesicle formation at morphologically distinct stages. *Mol. Biol. Cell* **12**, 2578-2589.

Deinhardt, K., Berninghausen, O., Willison, H. J., Hopkins, C. R. and Schiavo, G. (2006). Tetanus toxin is internalized by a sequential clathrin-dependent mechanism initiated within lipid microdomains and independent of epsin1. *J. Cell Biol.* **174**, 459-471.

Eggeling, C., Ringemann, C., Medda, R., Schwarzmann, G., Sandhoff, K., Polyakova, S., Belov, V. N., Hein, B., von Middendorff, C., Schonle, A. et al. (2008). Direct observation of the nanoscale dynamics of membrane lipids in a living cell. *Nature* **457**, 1159-1162.

Fantini, J., Garmy, N., Mahfoud, R. and Yahi, N. (2002). Lipid rafts: structure, function and role in HIV, Alzheimers and prion diseases. *Expert Rev. Mol. Med.* **2002**, 1-22.

Glebov, O. O., Bright, N. A. and Nichols, B. J. (2006). Flotillin-1 defines a clathrin-independent endocytic pathway in mammalian cells. *Nat. Cell Biol.* **8**, 46-54.

Gomez-Mouton, C., Lacalle, R. A., Mira, E., Jimenez-Baranda, S., Barber, D. F., Carrera, A. C., Martinez-A. C. and Manes, S. (2004). Dynamic redistribution of raft domains as an organizing platform for signaling during cell chemotaxis. *J. Cell Biol.* **164**, 759-768.

Gorodinsky, A. and Harris, D. A. (1995). Glycolipid-anchored proteins in neuroblastoma cells form detergent-resistant complexes without caveolin. *J. Cell Biol.* **129**, 619-627.

Goswami, D., Gowrishankar, K., Bilgrami, S., Ghosh, S., Raghupathy, R., Chadda, R., Vishwakarma, R., Rao, M. and Mayor, S. (2008). Nanoclusters of GPI-anchored proteins are formed by cortical actin-driven activity. *Cell* **135**, 1085-1097.

Hancock, J. F. (2006). Lipid rafts: contentious only from simplistic standpoints. *Nat. Rev. Mol. Cell Biol.* **7**, 456-462.

Haustein, E. and Schwille, P. (2003). Ultrasensitive investigations of biological systems by fluorescence correlation spectroscopy. *Methods* **29**, 153-166.

Hebbar, S., Lee, E., Manna, M., Steinert, S., Kumar, G. S., Wenk, M., Wohland, T. and Kraut, R. (2008). A fluorescent sphingolipid binding domain peptide probe interacts with sphingolipids and cholesterol-dependent raft domains. *J. Lipid Res.* **49**, 1077-1089.

Hooper, N. M. (1999). Detergent-insoluble glycosphingolipid/cholesterol-rich membrane domains, lipid rafts and caveolae (review). *Mol. Membr. Biol.* **16**, 145-156.

Jury, E. C., Flores-Borja, F. and Kabouridis, P. S. (2007). Lipid rafts in T cell signalling and disease. *Semin. Cell Dev. Biol.* **18**, 608-615.

Keller, P., Toomre, D., Diaz, E., White, J. and Simons, K. (2001). Multicolour imaging of post-Golgi sorting and trafficking in live cells. **3**, 140-149.

Lamaze, C., Dujeancourt, A., Baba, T., Lo, C. G., Benmerah, A. and Dautry-Varsat, A. (2001). Interleukin 2 receptors and detergent-resistant membrane domains define a clathrin-independent endocytic pathway. *Mol. Cell* **7**, 661-671.

Langhorst, M. F., Reuter, A. and Stuermer, C. A. (2005). Scaffolding microdomains and beyond: the function of reggie/flotillin proteins. *Cell Mol. Life Sci.* **62**, 2228-2240.

Langhorst, M. F., Reuter, A., Jaeger, F. A., Wippich, F. M., Luxenhofer, G., Plattner, H. and Stuermer, C. A. (2008). Trafficking of the microdomain scaffolding protein reggie-1/flotillin-2. *Eur. J. Cell Biol.* **87**, 211-226.

Lasserre, R., Guo, X. J., Conchonaud, F., Hamon, Y., Hawchar, O., Bernard, A. M., Soudja, S. M. H., Lenne, P. F., Rigneault, H., Olive, D. et al. (2008). Raft nanodomains contribute to Akt/PKB plasma membrane recruitment and activation. *Nat. Chem. Biol.* **4**, 538-547.

Le, P. U. and Nabi, I. R. (2003). Distinct caveolae-mediated endocytic pathways target the Golgi apparatus and the endoplasmic reticulum. *J. Cell Sci.* **116**, 1059-1071.

Lencer, W. I. and Saslowsky, D. (2005). Raft trafficking of AB5 subunit bacterial toxins. *Biochim. Biophys. Acta* **1746**, 314-321.

Lommerse, P. H., Vastenhoud, K., Pirinen, N. J., Magee, A. I., Spaink, H. P. and Schmidt, T. (2006). Single-molecule diffusion reveals similar mobility for the Lck, H-ras, and K-ras membrane anchors. *Biophys. J.* **91**, 1090-1097.

Macia, E., Ehrlich, M., Massol, R., Boucrot, E., Brunner, C. and Kirchhausen, T. (2006). Dynasore, a cell-permeable inhibitor of dynamin. *Dev. Cell* **10**, 839-850.

Mahfoud, R., Garmy, N., Maresca, M., Yahi, N., Puigserver, A. and Fantini, J. (2002). Identification of a common sphingolipid-binding domain in Alzheimer, prion, and HIV-1 proteins. *J. Biol. Chem.* **277**, 11292-11296.

Massol, R. H., Larsen, J. E., Fujinaga, Y., Lencer, W. I. and Kirchhausen, T. (2004). Cholera toxin toxicity does not require functional Arf6- and dynamin-dependent endocytic pathways. *Mol. Biol. Cell* **15**, 3631-3641.

Mayor, S. and Riezman, H. (2004). Sorting GPI-anchored proteins. *Nat. Rev. Mol. Cell Biol.* **5**, 110-120.

Mayor, S. and Pagano, R. E. (2007). Pathways of clathrin-independent endocytosis. *Nat. Rev. Mol. Cell Biol.* **8**, 603-612.

Neumann-Giesen, C., Falkenbach, B., Beicht, P., Claasen, S., Luers, G., Stuermer, C. A., Herzog, V. and Tikkanen, R. (2004). Membrane and raft association of reggie-1/flotillin-2: role of myristoylation, palmitoylation and oligomerization and induction of filopodia by overexpression. *Biochem. J.* **378**, 509-518.

Nichols, B. J., Kenworthy, A. K., Polishchuk, R. S., Lodge, R., Roberts, T. H., Hirschberg, K., Phair, R. D. and Lippincott-Schwartz, J. (2001). Rapid cycling of lipid raft markers between the cell surface and golgi complex. *J. Cell Biol.* **153**, 529-542.

Pagano, R. E., Puri, V., Dominguez, M. and Marks, D. L. (2000). Membrane traffic in sphingolipid storage diseases. *Traffic* **1**, 807-815.

Payne, C. K., Jones, S. A., Chen, C. and Zhuang, X. (2007). Internalization and trafficking of cell surface proteoglycans and proteoglycan-binding ligands. *Traffic* **8**, 389-401.

Pertz, O., Hodgson, L., Klemke, R. L. and Hahn, K. M. (2006). Spatiotemporal dynamics of RhoA activity in migrating cells. *Nature* **440**, 1069-1072.

Pinaud, F., Michalet, X., Iyer, G., Margeat, E., Moore, H. P. and Weiss, S. (2009). Dynamic partitioning of a glycosyl-phosphatidylinositol-anchored protein in glycosphingolipid-rich microdomains imaged by single-quantum dot tracking. *Traffic* **10**, 691-712.

Pol, A., Martin, S., Fernandez, M. A., Ingelmo-Torres, M., Ferguson, C., Enrich, C. and Parton, R. G. (2005). Cholesterol and fatty acids regulate dynamic caveolin trafficking through the Golgi complex and between the cell surface and lipid bodies. *Mol. Biol. Cell* **16**, 2091-2105.

Praefcke, G. J. K. and McMahon, H. T. (2004). The dynamin superfamily: universal membrane tubulation and fission molecules? *Nat. Rev. Mol. Cell Biol.* **5**, 133-147.

Roff, C. F., Goldin, E., Comly, M. E., Cooney, A., Brown, A., Vanier, M. T., Miller, S. P., Brady, R. O. and Pentchev, P. G. (1991). Type C Niemann-Pick disease: use of hydrophobic amines to study defective cholesterol transport. *Dev. Neurosci.* **13**, 315-319.

Saavedra, L., Mohamed, A., Ma, V., Kar, S. and de Chaves, E. P. (2007). Internalization of beta-amyloid peptide by primary neurons in the absence of apolipoprotein E. *J. Biol. Chem.* **282**, 35722-35732.

Sabharanjak, S., Sharma, P., Parton, R. G. and Mayor, S. (2002). GPI-anchored proteins are delivered to recycling endosomes via a distinct cdc42-regulated, clathrin-independent pinocytic pathway. *Dev. Cell* **2**, 411-423.

Sandvig, K., Spilsberg, B., Lauvrak, S. U., Torgersen, M. L., Iversen, T. G. and van Deurs, B. (2004). Pathways followed by protein toxins into cells. *Int. J. Med. Microbiol.* **293**, 483-490.

Schneider, A., Rajendran, L., Honsho, M., Gralle, M., Donnert, G., Wouters, F., Hell, S. W. and Simons, M. (2008). Flotillin-dependent clustering of the amyloid precursor protein regulates its endocytosis and amyloidogenic processing in neurons. *J. Neurosci.* **28**, 2874-2882.

Sever, S., Damke, H. and Schmid, S. L. (2000). Dynamin:GTP controls the formation of constricted coated pits, the rate limiting step in clathrin-mediated endocytosis. *J. Cell Biol.* **150**, 1137-1148.

Sharma, P., Varma, R., Sarasij, R. C., Ira Gousset, K., Krishnamoorthy, G., Rao, M. and Mayor, S. (2004). Nanoscale organization of multiple GPI-anchored proteins in living cell membranes. *Cell* **116**, 577-589.

Shogomori, H. and Futerman, A. H. (2001). Cholera toxin is found in detergent-insoluble rafts/domains at the cell surface of hippocampal neurons but is internalized via a raft-independent mechanism. *J. Biol. Chem.* **276**, 9182-9188.

Simons, K. and Gruenberg, J. (2000). Jamming the endosomal system: lipid rafts and lysosomal storage diseases. *Trends Cell Biol.* **10**, 459-462.

Solis, G. P., Hoegg, M., Munderloh, C., Schrock, Y., Malaga-Trillo, E., Rivera-Milla, E. and Stuermer, C. A. (2007). Reggie/flotillin proteins are organized into stable tetramers in membrane microdomains. *Biochem. J.* **403**, 313-322.

Steinert, S., Lee, E., Tresset, G., Zhang, D., Hortsch, R., Wetzel, R., Hebbar, S., Sundram, J. R., Kesavapany, S., Boschke, E. et al. (2008). A fluorescent glycolipid-binding peptide probe traces cholesterol dependent microdomain-derived trafficking pathways. *PLoS ONE* **3**, e2933.

Stuermer, C. A., Lang, D. M., Kirsch, F., Wiechers, M., Deininger, S. O. and Plattner, H. (2001). Glycosylphosphatidyl inositol-anchored proteins and fyn kinase assemble in noncaveolar plasma membrane microdomains defined by reggie-1 and -2. *Mol. Biol. Cell* **12**, 3031-3045.

Umemura, Y. M., Vrljic, M., Nishimura, S. Y., Fujiwara, T. K., Suzuki, K. G. N. and Kusumi, A. (2008). Both MHC class II and its GPI-anchored form undergo hop diffusion as observed by single-molecule tracking. *Biophys. J.* **95**, 435-450.

Wohland, T., Friedrich, K., Pick, H. A., Preuss Hovius, R. and Vogel, H. (2001). The characterization of a transmembrane receptor protein by fluorescence correlation spectroscopy. In *Single Molecule Spectroscopy: Nobel Conference Lectures* (ed. R. Rigler, M. Orrit and T. Basche), pp. 195-210. Berlin: Springer.

Wolf, A. A., Jobling, M. G., Wimer-Mackin, S., Ferguson-Maltzman, M., Madara, J. L., Holmes, R. K. and Lencer, W. I. (1998). Ganglioside structure dictates signal transduction by cholera toxin and association with caveolae-like membrane domains in polarized epithelia. *J. Cell Biol.* **141**, 917-927.